Chapter 3

Electrochemical Basis for EZSCAN/SUDOSCAN: A Quick, Simple, and Non-Invasive Method to Evaluate Sudomotor Dysfunctions

Hanna Ayoub, Jean Henri Calvet, Virginie Lair, Sophie Griveau, Fethi Bedioui and Michel Cassir

Additional information is available at the end of the chapter

http://dx.doi.org/10.5772/53965

1. Introduction

Globally, as of 2010, an estimated 285 million people had diabetes, with type 2 making up about 90% of the cases. Its incidence is increasing rapidly, and by 2030, this number is estimated to almost the double. Diabetes mellitus occurs throughout the world, but is more common (especially type 2) in the most developed countries. The greatest increase in prevalence is, however, expected to occur in Asia and Africa, where most patients will probably be found by 2030. The increase in incidence in developing countries follows the trend of urbanization and lifestyle changes, perhaps most importantly a "Western-style" diet [1].

All forms of diabetes increase the risk of long-term complications. These typically develop after many years (10–20), but may be the first symptom among those which have otherwise not received a diagnosis before that time. The major long-term complications relate to damage to blood vessels. Diabetes doubles the risk of cardiovascular diseases. The main "macrovascular" diseases (related to atherosclerosis of larger arteries) are ischemic heart disease (angina and myocardial infarction), stroke and peripheral vascular disease. Diabetes also causes "microvascular" complications as damage to the small blood vessels [2]. Diabetic retinopathy, which affects blood vessel formation in the retina of the eye, can lead to visual symptoms, reduced vision, and potentially blindness. Diabetic nephropathy, the impact of diabetes on the kidneys, can lead to scarring changes in the kidney tissue, loss of small or progressively larger amounts of protein in the urine, and eventually chronic kidney disease requiring dialysis. Diabetic neuropathy is the impact of diabetes on the nervous system, most commonly causing numbness, tingling and pain in the feet and also increasing the risk

of skin damage due to altered sensation. Together with vascular disease in the legs, neuropathy contributes to the risk of diabetes-related foot problems (such as diabetic foot ulcers) that can be difficult to treat and occasionally require amputation. Peripheral neuropathy is the most prevalent complication of type 2 diabetes. The 2004 National Health and Nutrition Examination Survey (NHANES) on lower extremity complications revealed that close to 10% of people with diabetes have peripheral arterial disease, but close to 30% have neuropathy. The survey also showed that over 7% have an active foot ulcer, a frequent cause of hospitalization and a common pathway to amputation [3].

Peripheral neuropathy is often recognized by patients or their physicians at a time when symptoms outweigh physical signs. Sensory symptoms, paresthesias, sensory loss, and neuropathic pain are common initial complaints. Although injury to small fiber calibers and types occurs, small-diameter unmyelinated or lightly myelinated nociceptive and autonomic fibers are often prominently affected in these common neuropathies. There is an increasing interest in recognizing and treating neuropathy early in its course. Sweat glands are innervated by the sudomotor, postganglionic, unmyelinated cholinergic sympathetic C-fibers that are thin and can be damaged very early in diabetes. Sudomotor dysfunction may result in dryness of foot skin and has been associated with foot ulceration. Assessment of sudomotor dysfunction contributes to the detection of autonomic dysfunction in diabetic peripheral neuropathy and American Diabetes Association suggests that sudomotor function assessment of small fiber status should be included in the diagnostic tests for the detection of neuropathies in diabetes. The quantitative sudomotor axon reflex test (QSART) is capable of detecting distal small fiber polyneuropathy and may be considered the reference method for the detection of sudomotor dysfunction [4]. Other available techniques for assessment of sudomotor function include the thermoregulatory sweat test, silastic imprint method, the indicator plaster method. But these tests are time consuming and highly specialized tests so they are mainly used for research purposes. Skin biopsies have been developed to assess small C-Fibers. Recently, this method has been improved by assessment of small C-Fibers that innervate sweat glands. However, this method is invasive [5].

The management of diabetes alone renders considerable expenditure, however macrovascular and microvascular complications are the major cause of healthcare costs. Data from a United States study indicate that renal and cardiovascular complications seem to be the most prevalent and are associated with particularly high costs. In this study abnormal renal function and end-stage renal disease were shown to vastly increase costs of diabetes treatment, up to 771%. Furthermore, an analysis of several individual studies showed that atherosclerosis in Type 2 diabetes accounted for approximately one third of the total healthcare costs related to the disease. In a study of patients with myocardial infarction (MI), patients with diabetes had a higher per-patient total direct medical charge (inclusive of initial hospitalisation) compared to patients without diabetes.

In 2000, it was estimated that 25% of overweight adults aged 45-74 years had prediabetes, which translates into about 12 million persons in the U.S. Furthermore, in the process of identifying those with prediabetes, it was estimated that an additional 6.5 million persons with undiagnosed diabetes would have been detected. Recent controlled trials on diabetes

http://dx.doi.org/10.5772/53965

prevention have confirmed that lifestyle changes such as diet, weight loss, and exercise as well as the drug metformin can substantially delay or prevent the progression from impaired metabolism to type 2 diabetes. Thus, several million individuals could benefit from diabetes prevention intervention [6].

There is a need to diagnose subjects with high risk for diabetes or cardiovascular diseases at an earlier stage using a simple, non-invasive, sensitive, quick and inexpensive tool. Presently, prediabetes and diabetes are diagnosed by blood glucose or HbA_{1C} levels with threshold values that were initially based on risk for retinopathy, a microvascular complication. Based on studies performed with QSART or skin biopsies, small fiber neuropathy has been shown to develop early in patients with prediabetes or cardiometabolic risk. However, these two highly specialized methods cannot be used for a large screening.

2. Principle of the method

EZSCAN/SUDOSCAN is a device (Figure 1) recently developed to provide an accurate evaluation of sweat gland function [7]. Patients place their hands and feet on electrodes, placed on skin region with a high density of sweat glands, and an incremental low direct voltage (lower than 4 V) is applied during a two minute interval. Electro-sweat conductance (ESC) is then calculated from the resulting voltage and the generated current, which is expressed in three ways: (i) current as a function of the anodic potential (so-called E), (ii) current as a function of the absolute values of the cathodic potential after applying an incremental voltage at the anode (so-called V), and (iii) current as a function of U = E+V. It is a dynamic method allowing evidence of sweat dysfunction not detectable in physiological conditions. Quantitative results are expressed as ESC, in microsiemens, μS) for the hands and feet, and a risk score is derived from the ESC values and demographic data.

3. Clinical studies for the evaluation of the performances of the device

Several studies were performed to demonstrate the robustness of the method followed by a proof of concept study and to validate the use of the EZSCAN/SUDOSCAN in detection of diabetes complications and in screening of prediabetes [8].

a. Symmetry

As the commonest form of diabetic neuropathy is symmetric, it was important to ensure that ESC measurements between right and left side were comparable. In this way, ESC in hands and feet were compared between right and left side to assess agreement between both sides using a Bland-Altman plot [9]. Coefficient of variation calculated on 1365 subjects was 3% for hands and 2% for feet, between right and left side.

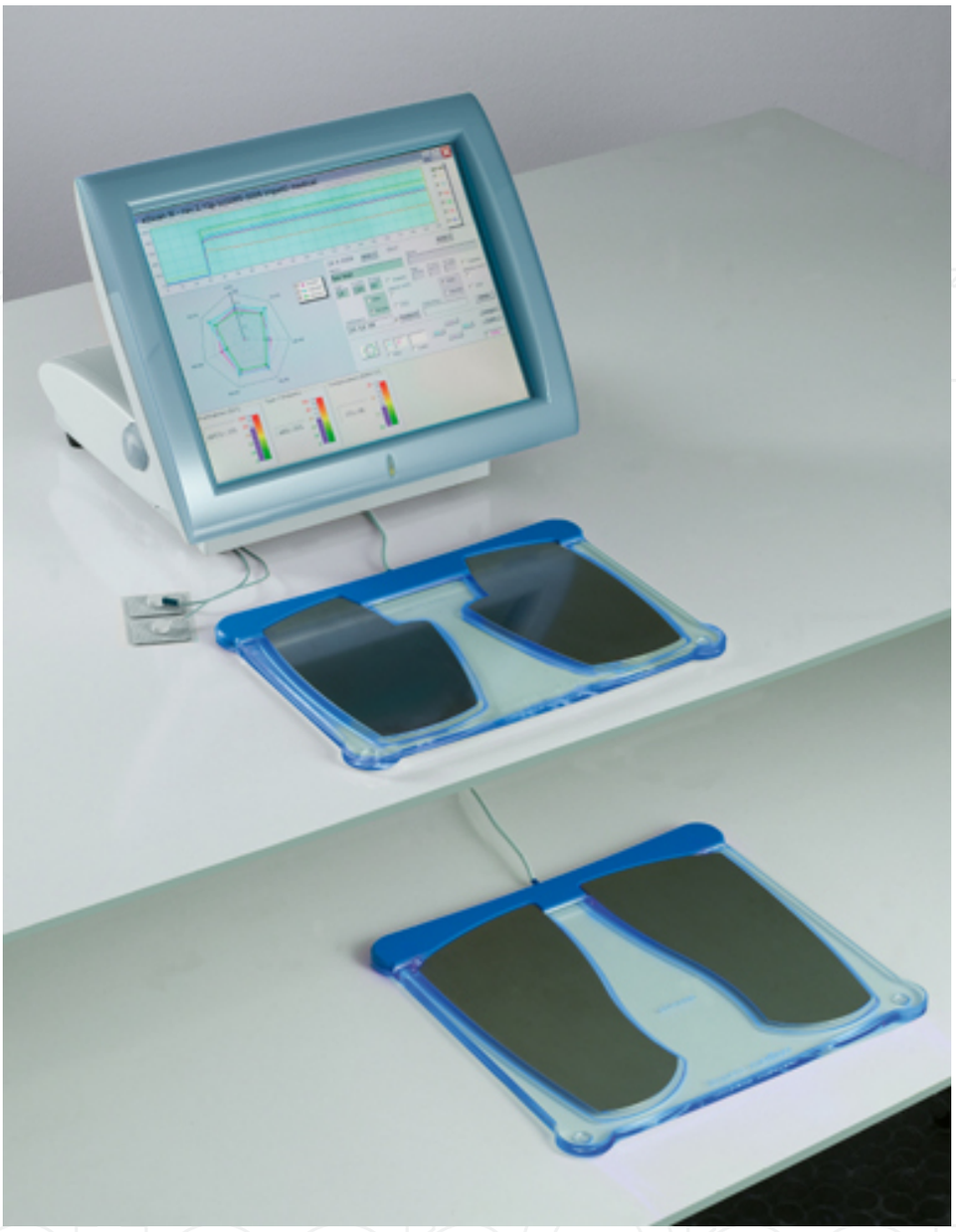

Figure 1. Photo of the device: screen and electrodes.

b. Gender effect

No significant difference was observed in ESC measured in hands and feet between female and male subjects involved in the studies or surveys performed [8].

c. Reproducibility

Measurements were assessed twice in the same day in patients with at least one cardiovascular risk and in patients with diabetes. Results were compared using a Bland-Altman plot [9]. The coefficient of variation was 7% in hands and 5% in feet in patients with cardiovascular risk and 15% in hands and 7% in feet in patients with diabetes. Co-

http://dx.doi.org/10.5772/53965

efficient of variation for glycemia, which is a gold standard for diabetes, between the two measurements was 32%.

d. Effects of glycemia

This technology has to be used in patients with prediabetes or diabetes, with potential high variations in glycemia. Thus, it was important to ensure that measurements were not influenced directly by glycemia itself. Thus, measurements were performed with a set of ten patients when their glycemia was greater than 18 mM/L and compared with measurements performed in the same patients when glycemia was below 6 mM/L. Coefficient of variation from a Bland and Altman plot with or without hyperglycemia was 10% for foot ESC.

e. Diagnosis of diabetes complications

- Screening of peripheral neuropathy

Perturbation of pain sensation is considered as one of the major initiating risk factors for diabetic foot ulcer. Sweat dysfunction leading to abnormal skin conditions including dryness and fissures could increase the risk of foot ulcers. The aim of this study was to evaluate SUDOSCAN as co-indicator of severity of diabetic polyneuropathy. 142 patients with diabetes (age 62 ± 18 years, diabetes duration 13 ± 14 years, HbA_{1c} 8.9 ± 2.5%) were measured for vibration perception threshold (VPT) using a biothesiometer and for sudomotor dysfunction by measuring ESC. Feet ESC showed a descending trend from 66 ± 17 μS to 43 ± 39 μS corresponding to an ascending trend of VPT threshold from < 15 V to > 25 V ($p = 0.001$). Correlation between VPT and ESC was -0.45 ($p < 0.0001$). Foot ESC was lower in patients with fissures while VPT was comparable. Both VPT and foot ESC were correlated with retinopathy status [10].

- Screening of cardiovascular autonomic neuropathy

Cardiovascular Autonomic Neuropathy (CAN) is a common but overlooked complication of diabetes. SUDOSCAN was compared to Heart Rate Variability (HRV) and to Ewing tests, known to be reliable methods for the investigation of CAN.

232 patients with diabetes were measured for HRV at rest and during moderate activity (stair climbing). Time and frequency domain analysis techniques, including measurement of Standard Deviation of the average beat to beat intervals (SDNN) over 5 minutes, High Frequency domain component (HF) and Low Frequency domain component (LF), were assessed during HRV testing. Heart rate variations during deep breathing and heart rate and blood pressure responses while standing, as described by Ewing according to the recommendations of the French Health Authority were also assessed. ESC was measured on the hands and feet, and a risk score was calculated. Patients were classified according to their risk score. The classifications were as follow: no sweat dysfunction, moderate sweat dysfunction and high sweat dysfunction. All results are means ± SD.

The highest correlation was observed between the risk score based on sudomotor function and the LF component during moderate activity ($r = 0.47$, $p < 0.001$). The risk score was higher in patients with a LF component value during moderate activity of < 90 ms^2 (1^{st} quartile)

when compared to LF > 405 ms^2 (3^{rd} quartile) (46 ± 13 vs. 30 ± 13, $p < 0.001$). The risk score based on sweat function was higher in patients with 2 abnormal Ewing tests when compared to patients with all tests normal (47 ± 12 vs. 34 ± 14, $p < 0.001$). When taking two abnormal Ewing tests as reference the AUC (air under curve) of the Receiver Operating Characteristic (ROC) curve for this risk score was 0.74 with a sensitivity of 92% and a specificity of 49% for a risk score cut-off value of 35%. Regarding ROC curve analysis when choosing LF power component during moderate activity at a threshold of 90 ms^2 (1^{st} quartile) as reference, the AUC was higher for SUDOSCAN risk score (0.77) compared to standards Ewing tests : E/I ratio (0.62), 30:15 ratio (0.76) and blood pressure change to standing (0.65). Using a cut-off of 35%, for SUDOSCAN risk score sensitivity and specificity were respectively 88% and 54% [11].

- Screening of diabetic nephropathy

Given the inter-relationships between dysglycemia, vasculopathy and neuropathy, it was hypothesized that SUDOSCAN may detect diabetic kidney disease (DKD).

In a case-control cohort consisting of 50 Chinese type 2 diabetic patients without DKD (ACR < 2.5mg/mM in men or ACR < 3.5mg/mM in women and eGFR > 90 ml/min/1.73 m^2) and 50 with DKD (ACR ≥ 25 mg/mM and eGFR < 60ml/min/1.73 m^2), we used spline analysis to determine the threshold value of SUDOSCAN score to predict DKD and its sensitivity and specificity.

SUDOSCAN scores were highly correlated with log values of eGFR ($r = 0.67$, $p < 0.0001$, see Figure 2) and ACR ($r = -0.66$, $p < 0.0001$). Using a cutoff value of 55 on the risk score scale, the score had 94% sensitivity and 78% specificity to predict DKD with a likelihood ratio of 4.2, positive predictive value of 81% and negative predictive value of 93%. In patients without DKD, those with low SUDOSCAN score (n = 10) had longer disease duration [median (IQR): 13 (9-17) vs. 8 (4-16) years, p=0.017] and were more likely to have retinopathy (36.7% vs. 5.1%, p=0.02), lower eGFR [98 (95.00-103) vs. 106 (98.5-115), $p = 0.036$] and more treated with RAS blockers (81.8% vs. 25.6%, $p = 0.002$) than those with normal score. On multivariable analysis, SUDOSCAN score remained an independent predictor for DKD (1= yes, no = 0) ($\beta = -0.72$, $p = 0.02$) along with smoking ($\beta = -2.37$, $p = 0.02$), retinopathy ($\beta = 3.019$, $p = 0.01$), triglyceride ($\beta = 2.56$, $p = 0.013$) and blood hemoglobin ($\beta = -0.613$, $p = 0.04$) [12].

f. Proof of concept study

As sweat chloride movements in sweat ducts are likely to be impaired in cystic fibrosis (CF), SUDOSCAN results were compared in CF patients and control subjects. ESC, measured when a very low voltage is applied, and dESC, difference between ESC at very low voltage and ESC at low voltage, were assessed in 41 adult patients with classical CF and 20 healthy control subjects.

ESC measurements on hands and feet were significantly higher in CF patients as compared to control subjects. dESC was significantly lower in CF patients and more discriminative (9 ± 18 μS vs. 49 ± 31 μS, $p < 0.0001$ on hands and 34 ± 24 μS vs. 93 ± 24 μS, $p < 0.0001$ on feet) (see Figure 3 for an individual comparison). dESC measurement provided a diagnostic specifici-

http://dx.doi.org/10.5772/53965

ty of 1 and a sensitivity of 0.93. Correlation between feet ESC and sweat chloride concentration as measured by sweat test was -0.70 ($p < 0.0001$). Precision for the measurements was 6% for hands ESC, 4% for feet ESC, 9% for hands dESC and 3% for feet dESC [13].

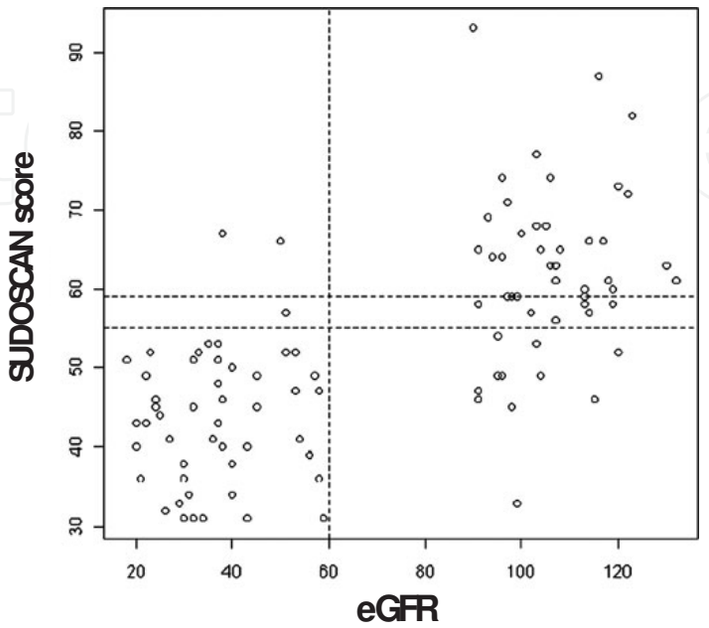

Figure 2. A scatter plot and grid analysis showing the correlations between estimated glomerular filtration rate (eGFR) and EZSCAN scores [adapted from 12].

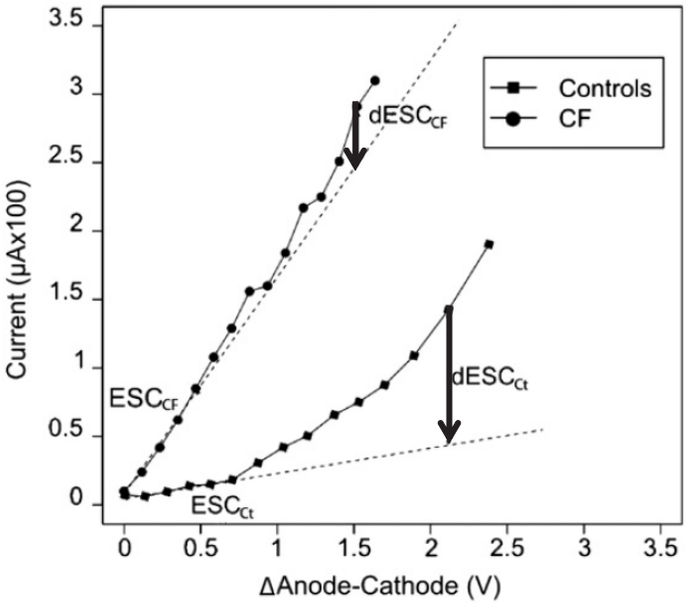

Figure 3. Individual current-voltage current curves for a control subject and a patient with cystic fibrosis showing dESC, the difference between ESC at low voltage and at high voltage dESC is shown by the up down arrow.

g. Identification of subjects at high risk of diabetes

A longitudinal study was performed in subjects with an initial normal glucose tolerance (NGT) to assess the ability of EZSCAN to predict future abnormalities in glucose tolerance.

South Asian (Indian) subjects (n = 69, 48% male, mean age 42 ± 9 years, mean BMI 28 ± 5 kg/m^2) diagnosed as NGT with a previous oral glucose tolerance test (OGTT, T0) underwent a frequently sampled OGTT (FSOGTT), 8 months later (T8) with calculation of the area under the curve (AUC) for glucose and insulin. At both times EZSCAN tests were done. Using $AUC_{glucose}$ and $AUC_{insulin}$ measured by the FSOGTT, subjects were categorised as normal, high $AUC_{insulin}$ or isolated high $AUC_{glucose}$. Odds ratio (OR) for having high $AUC_{insulin}$ or isolated high $AUC_{glucose}$ vs. normal was computed by logistic regression analysis using EZSCAN risk classification at T0 as independent variable (< 50% = normal, no risk, 50-65% = intermediate risk and > 65% = high risk).

At T8, 11 and 5 subjects developed impaired glucose tolerance and diabetes respectively. OR of having high $AUC_{insulin}$ or isolated high $AUC_{glucose}$ in the different risk groups was 6.19 (CI 95% 1.50– 25.48, p = 0.0116) for high risk vs. no risk and 3.0 (CI 95% 0.98–9.19, p = 0.0545) for intermediate risk vs. no risk. Sensitivity of EZSCAN for early detection of these abnormalities in glucose tolerance was 77% while it was 14% for fasting plasma glucose and 66% for HbA_{1C} [14].

h. Conclusion on clinical studies

All these clinical studies that have been published in international peer reviewed journals evidenced that sweating status as assessed by EZSCAN/SUDOSCAN:

- is a robustness method with good reproducibility
- is a sensitive method when compared with the conventional methods may be very useful to identify and manage subjects at risk for developing glucose intolerance
- may be a quantitative indicator on the severity of polyneuropathy that may be useful for the early prevention of foot skin lesions
- may be used for the early screening of cardiovascular autonomic neuropathy in daily clinical practice before more sophisticated, specific, and time-consuming tests
- may be used to detect high risk subjects for diabetic kidney diseases

This quick and simple method is well accepted by the subject, does not require specific preparation and does not need high training allowing its performance by non specialized teams.

4. *In-vitro* study

Experiments were performed *in-vitro* to improve the method and to understand: i) the role of the components of the sweat in electrochemical reaction with nickel; ii) the onsets of currents observed in clinical studies and the influencing factors; iii) the electrochemical kinetics

http://dx.doi.org/10.5772/53965

of reactions; iv) the effect of ageing of electrodes; v) the consequences on electrochemical reaction of the use of stainless-steel electrodes generally recommended for medical use.

4.1. Electrochemical characterization of nickel electrodes in phosphate and carbonate electrolytes

Although the electrochemical properties of nickel have been widely examined, through the analysis of its corrosion in aqueous acid or alkaline solution, very few studies have been dedicated to the specific assessment of its behavior in physiological solutions. In a preliminary study, we thoroughly explored the electrochemical behavior of nickel electrode (i) in a three-electrode set-up combining a nickel counter electrode and a nickel pseudo-reference electrode in order to mimic the whole Ni electrode configuration of the SUDOSCAN™ device; (ii) and in synthetic buffered phosphate and carbonate solutions (PBS and CBS) in which the pH and the concentrations of chloride, lactate and urea were varied to mimic the behavior of the electrodes in contact with sweat.

This approach provides insight into the origin of the onset of responses measured upon the application of low voltage potential with variable amplitudes to Ni electrodes. This study also constitutes a sound approach aimed at understanding the chemical key parameters controlling the electrochemical currents.

- **Anodically:** for low voltage amplitude, the electrochemical reactions measured at the electrodes are mainly those related to the oxidation of Ni leading to the formation of an oxy-hydroxide film [15]. The following reactions have been proposed for Ni oxidation in presence of Cl^- [16,17]:

$$Ni + H_2O = Ni(H_2O)_{ad} = Ni(OH)_{ad} + H_{aq}^{+} + e^{-}$$

$$Ni(H_2O)_{ad} + Cl^- = Ni(ClOH)^-_{ad} + H^+ + e^-$$

$$Ni(OH)_{ad} + H^+ = Ni^{2+}_{aq} + (H_2O)_{ad} + e^- = Ni(OH)_2$$

At high potentials, the breakdown of the oxy-hydroxide film becomes the main anodic reaction [15]. This is mainly due to the competitive adsorption between Cl^-, oxygen containing species, carbonate anions and the formation of soluble species as Ni-Cl- and/or NiO(H)-Cl- leading to the breakdown of the oxy-hydroxide film. This could also be due to the direct penetration of chloride ions through the oxy-hydroxide film. Therefore, the increase in the concentration ratios $[Cl^-]/[OH^-]$ acts in favor of the adsorption of Cl^- and, thus, the weakness of the passive layer occurs, leading to its breakdown at low potential values.

- **Cathodically:** for low voltage amplitude, the electrochemical reactions are mainly related to the reduction of the oxy-hydroxide film. The following reactions have been proposed:

$$NiO + 2H^+ + 2e^- \rightarrow Ni + H_2O$$

And/or

$$Ni(OH)_2 + 2H^+ + 2e^- \rightarrow Ni + 2H_2O$$

At high voltage potential, the reduction of the oxy-hydroxide film and the electrolytic solution govern the cathode reactions [15].

In the particular case of CBS (36 mM, pH 6.4) containing different concentrations of chloride ions, within the expected range of Cl^- concentration in sweat, the positive potential going direction of the cyclic voltammograms (Figure 4) show that in all cases, an anodic plateau appears at ca. 0.3 V, indicating the formation of a passive film composed probably by $Ni(OH)_2$ and/or NiO.

In this examined range of potentials, the voltammograms show also a large anodic current at high potentials due to the localized dissolution of the nickel following Cl^- attack. The increase in the concentration of Cl^- initiates earlier the localized dissolution of Ni. Indeed, the breakdown potential "E_b" shifts towards lower anodic potentials when increasing the concentration of Cl^-.

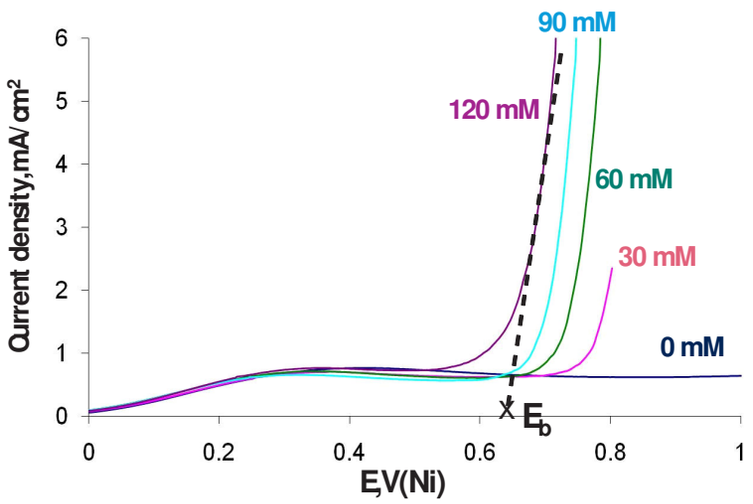

Figure 4. Cyclic voltammograms of Ni electrode in aerated CBS (36 mM; pH 6.4) in presence of different concentration of NaCl. Scan rate: 100 mV/s [adapted from 15].

Moreover, the variation of buffer, urea and lactate concentrations does not have a significant effect on the electrochemical anodic behavior of Ni and notably on the breakdown potential "E_b". Therefore, the anodic currents are likely to be controlled by the variation of Cl^- concentration [15,18].

The obtained results (data not show) indicate that the cathodic currents are less affected by the variation of the electrolyte concentrations and they are likely to be controlled by the variation of pH value.

4.2. Comparison of *in-vitro* results and clinical observations

In order to establish a parallel between the *in-vitro* observations and those obtained during the clinical tests to further understand the origin of the onsets of currents and their evolution with chloride ion concentrations, linear anodic voltammograms were performed. The

http://dx.doi.org/10.5772/53965

induced potentials on the counter electrode (playing the role of cathode in this case) were measured simultaneously. The results are then expressed, as in the medical technology (Figure 5), as follows: (1) I vs. E, (2) I vs. V and (3) I vs. U (= E+V) where I is the current.

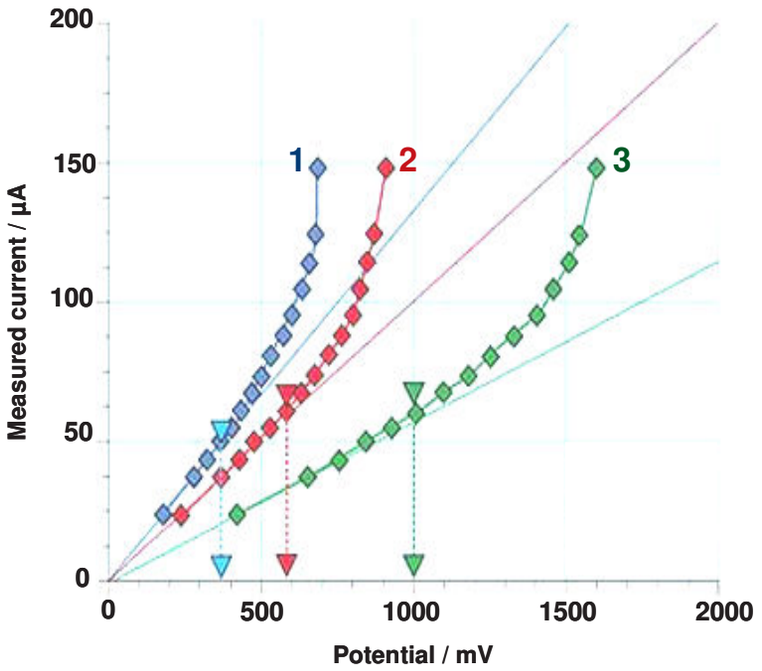

Figure 5. Example of the electrochemical results obtained by the SUDOSCAN technology (1: I vs. E; 2: I vs. V; and 3: I vs. U = E+V).

As shown above, the variation of chloride concentration is the main sweat parameter affecting the anodic electrochemical behavior of Ni. This led us to study the influence of the concentrations of Cl^- on the measured variation of current-voltage outputs. Linear anodic voltammograms were performed in (I) -0.3 V to 0.9 V vs. SCE potential range and the induced potentials on the counter electrode (playing the role of cathode in this case) were measured simultaneously. The results are then expressed, as in SUDOSCAN™ technology.

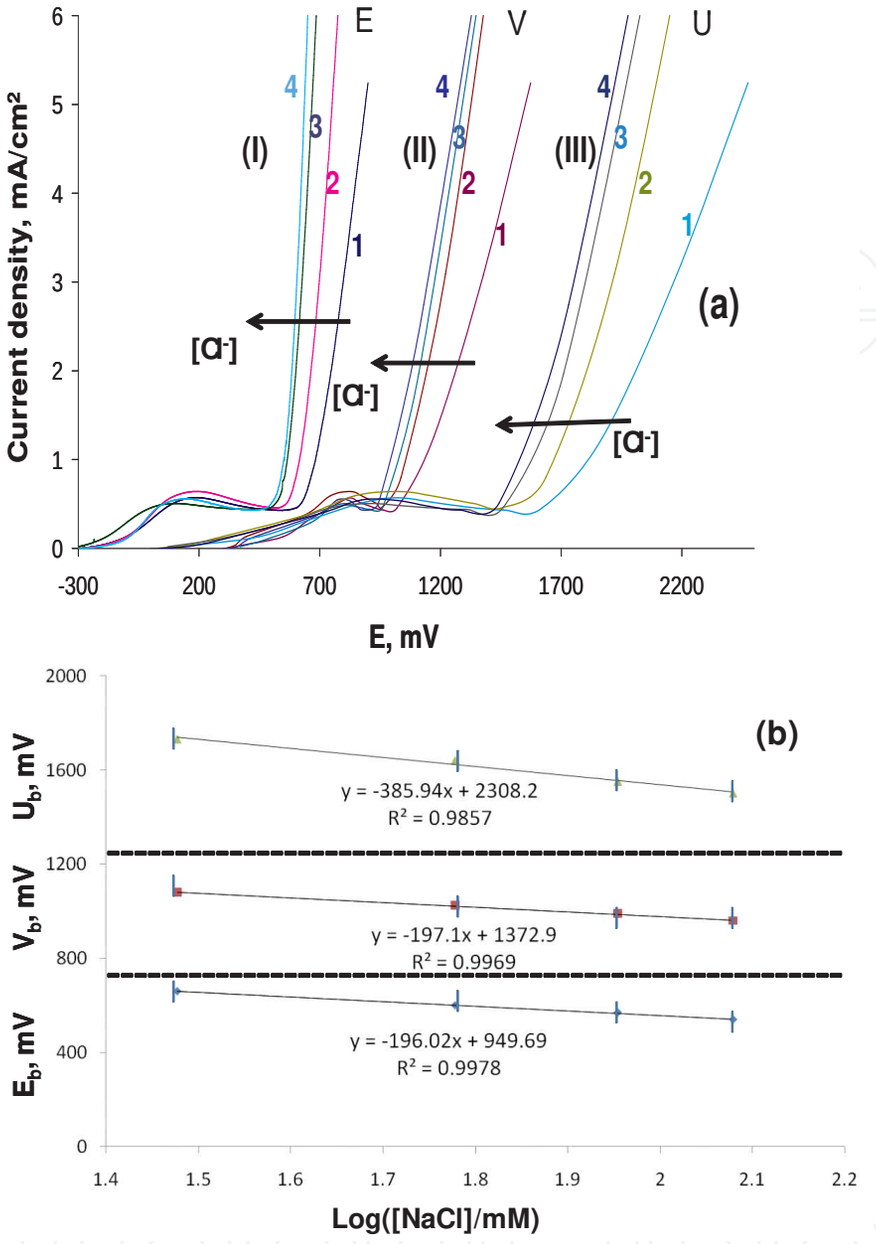

Figure 6. a) (I) j vs. E, (II) j vs. V, and (III) j vs. U (= E+V), where j is the current density, after sweeping the potential between -0.3 V → 0.8 V vs. SCE in CBS (36 mM, pH 7) and in presence of NaCl (curves 1: 30 mM, curves 2: 60 mM, curves 3: 90 mM, and curves 4: 120 mM). (b) Evolution of E_b, V_b and U_b as a function of Log[Cl^-] (data from Figure 6a) [adapted from 19].

In the particular case of pH 7, Figure 6a depicts the results obtained in CBS (36 mM, pH 7), containing different concentrations of NaCl (30, 60, 90, and 120 mM). It clearly appears that the concentration of Cl^- affects the variation of the current as a function of E, V and U. In fact, the increase in the concentration of Cl^- shifts linearly the breakdown potential, E_b, towards more cathodic values, as it can be seen in Figure 6b. According to the same way than E_b, V_b and U_b can be also evaluated as the potentials associated to the point of deviation of j-V and j-U curves. Figure 6b shows that the increase in the concentration of Cl^- shifts linearly

http://dx.doi.org/10.5772/53965

E_b and V_b towards lower V values and the slope value of V_b vs. Log[Cl^-] is close to that of E_b vs. Log[Cl^-]. Consequently, the increase in Cl^- concentration shifts linearly U_b towards lower U values and the slope of U_b vs. Log[Cl^-] is about twice the value found for E_b or V_b vs. Log[Cl^-]. It should be noted that the results obtained at pH 6 provided the same features as in the present case. This implies that the evolution of the current-voltage curves reported in Figures 6a and 6b are not very sensitive to the variation of pH values.

Furthermore, curves obtained for generated current as a function of E, V, U during clinical tests are quite comparable (Figure 5 and 6a). These results led us to conclude that the determination of the current curve as a function of the potential (anode, cathode or their difference) provides a very efficient way to detect the deviation in the ion balance and notably the deviation in Cl^- concentration at the level of the electrodes.

4.3. Electrochemical kinetics of anodic nickel dissolution

As shown above, the variation of chloride ion concentration plays a key role in predicting sudomotor dysfunction by controlling the generated current at high anodic potentials, notably the currents related to the localized anodic dissolution of nickel. This led us to study the kinetics of the different electrochemical reactions related to the localized dissolution of nickel in carbonate buffer solutions (CBS) at different physiological pH values and in presence of different concentrations of chloride ions, within the expected range of concentrations in sweat at rest. This aims at studying the mechanisms of the electrochemical reactions and completing a theoretical model on the basis of the electrical signals registered during the clinical tests. Our results show that in a pH range between 5-7, the rate determining step appears to be the transfer of a first one-electron, as suggested by Tafel slopes close to 0.120 V/decade. However, the reaction order in chloride ions changes from around 2, for pH 7, to around 1, for pH values between 6 and 5 without a change in the rate-determining step [20].

At pH 7, the following mechanism has been proposed for the reactions taking place before and during the rate determining step (rds):

1. $Ni + 2Cl^- \leftrightarrows [NiCl_2]^{2-}_{ads}$

2. $[NiCl_2]^{2-}_{ads} \leftrightarrows [NiCl_2]^- + e^-$ rds

And at pH 5-6, the following mechanism has been proposed:

1. $Ni + Cl^-(aq) \leftrightarrows Ni(Cl^-)_{ads}$

2. $Ni(Cl^-)_{ads} \leftrightarrows Ni(I)Cl + e^-$ rds

4.4. Effect of electrode ageing on measurements

The nickel electrodes play alternately the role of anode and cathode, which do not undergo any specific pretreatment before each measurement. Thus, the analysis of the temporal evolution of the physico-chemical properties of nickel is of prime importance to ensure the good performance of the medical device. The objectives of the present work are to study both the

electrochemical behavior and the surface chemical composition of nickel electrodes after ageing under repeated cyclic voltammograms in different potential windows. Surface chemical characterizations by XPS (X-ray photoelectron spectroscopy) and ToF-SIMS (Time of Flight-Secondary Ion Mass Spectrometry) were performed on nickel electrodes after ageing with repeated cyclic voltammograms in carbonate buffer solutions containing the main components of sweat, at different potential ranges, in: (i) a restricted anodic potential range; (ii) a negative extended potential range.

The electrochemical behavior of Ni electrodes was first studied after ageing with repeated cyclic voltammograms in a potential range of -0.3 V to 0.5 V and return to -0.3 V (anodic region only). Then, in order to assess the influence of alternating the polarity of the electrodes during the clinical tests on the Ni ageing behavior (each electrode playing alternately the role of anode or cathode), successive cyclic voltammograms were performed in a potential range of -0.3 V → 0.5 V → -1 V (cathodic region). All the experiments were conducted in aerated CBS solutions, with a concentration of 120 mM of NaCl.

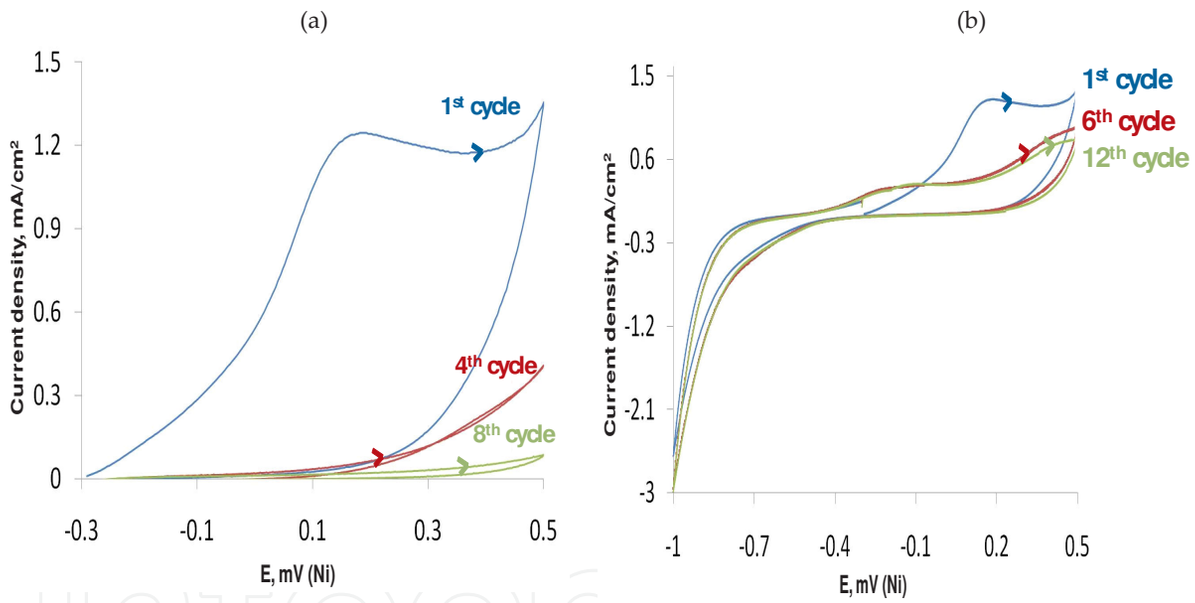

Figure 7. Successive cyclic voltammograms of Ni electrode in CBS (pH 6.4) in presence of 120 mM NaCl. Scan rate: 100 mV/s. (a) potential range: -0.3 V → 0.5 V → -0.3 V and (b) potential range: -0.3 V → 0.5 V → -1.0 V [adapted from 21].

Figure 7a shows cyclic voltammograms after 1, 4 and 8 cycles in aerated CBS (36 mM) in presence of Cl^- (120 mM) in the potential range [-0.3 V → 0.5 V → -0.3 V]. It clearly appears that the first potential sweep strongly affects the subsequent cyclic voltammograms. The anodic plateau of the first cycle, attributed to Ni oxidation, is no longer observed in the following cycles (see, for example, the voltammograms of the fourth cycle and eighth cycles in Figure 7a). These changes in the voltammograms are mainly attributed to the formation of an oxide layer firmly attached to the metal and forming a compact barrier between the metal and the solution with a very low electronic conductivity during the first cycle [22].

http://dx.doi.org/10.5772/53965

Figure 7b shows the obtained cyclic voltammograms after 1, 6 and 12 cycles when the potential on the return cycle is extended to -1 V (potential range [-0.3 V → 0.5 V → -1 V → -0.3 V]). Contrarily to the results presented in Figure 7a, there are two new observations: (i) the Ni oxidation process is still observed during the subsequent cycles around -0.4 V and 0.4 V, (ii) the high intensities of the anodic current remain with the subsequent cycles. This is mainly due to a partial reduction or re-activation [22,23] of the compact oxide film when the potential scan is extended down to -1 V. The re-activation of the oxide film, in the cathodic reduction step, is probably due to a surface modification or post-electrochemical re-organization of the initial deposited species [24] leading to an increase in the electronic conductivity of the surface of the Ni electrode.

It should be noted here that additional experiments, performed in the absence of Cl^-, displayed the same features as in the present case (data not shown). This implies that the voltammograms reported in Figure 7 are poorly sensitive towards the presence of Cl^-, as the potential range is well below the pitting corrosion one.

XPS characterizations were performed on the series of samples shown in Figures 7a-b. The Ni $2p_{3/2}$ core levels were systematically decomposed into the spectroscopic contributions characteristic of metallic nickel (main peak located at a BE of 852.8 ± 0.2 eV, nickel plasmon at 856.3 ± 0.2 eV and satellite at 858.8 ± 0.2 eV [25-27]), nickel oxide NiO (main peak located at 854.7 ± 0.2 eV and two satellites located at 856.4 ± 0.2 eV and 861.7 ± 0.2 eV [25-27]) and $Ni(OH)_2$ (main peak at 856.7 ± 0.2 eV and satellite at 862.6 ± 0.2 eV [26,27]). Figure 8 displays these core levels and their decomposition into individual contributions of Ni, NiO, and $Ni(OH)_2$.

Based on previously published data, a simple layer model of the passive film can be suggested. It is composed of an homogeneous continuous outermost layer of $Ni(OH)_2$ and an homogeneous continuous inner NiO oxide layer, in contact with the metal [28,29].

It was possible to calculate the equivalent thicknesses of the $Ni(OH)_2$ and NiO layers, as well as the total oxidized surface layer (as the arithmetic sum of the two former ones), from the peak intensities of the fitted Ni $2p_{3/2}$ core levels, taking into account such two-layer model for the description of the Ni oxide film (see Equations 1 and 2) in all experiments. The values are reported in Table 1.

$$d_{NiO} = \lambda_{Ni}^{NiO}.\sin\beta.\ln\left[1+\frac{D_{Ni}^{Ni}.\lambda_{Ni}^{Ni}}{D_{Ni}^{NiO}.\lambda_{Ni}^{NiO}}\cdot\frac{I_{Ni}^{NiO}}{I_{Ni}^{Ni}}\right] \quad (1)$$

$$d_{Ni(OH)_2} = \lambda_{Ni}^{Ni(OH)_2}.\sin\beta.\ln\left[1+\frac{D_{Ni}^{Ni}.\lambda_{Ni}^{Ni}}{D_{Ni}^{Ni(OH)_2}.\lambda_{Ni}^{Ni(OH)_2}}\cdot\frac{I_{Ni}^{Ni(OH)_2}}{I_{Ni}^{Ni}}\cdot\exp\left(\frac{-d_{NiO}}{\lambda_{Ni}^{NiO}.\sin\beta}\right)\right] \quad (2)$$

Where d is the layer thickness, β is the take-off angle of the photoelectrons with respect to the sample surface, λ_M^N is the inelastic mean free path of the photoelectrons coming

from M in the matrix N, I_{Ni}^{Ni} is the nickel intensity for NiO in the bulk metal, $I_{Ni}^{Ni(OH)_2}$ is the nickel intensity for $Ni(OH)_2$, D_M^N is the density of M in the matrix N, the inelastic mean free paths used in this work are the following: 1.41 nm for λ_{Ni}^{Ni} [26], 1.43 nm for λ_{Ni}^{NiO} [26] and 1.19 nm for $\lambda_{Ni}^{Ni(OH)_2}$ [26].

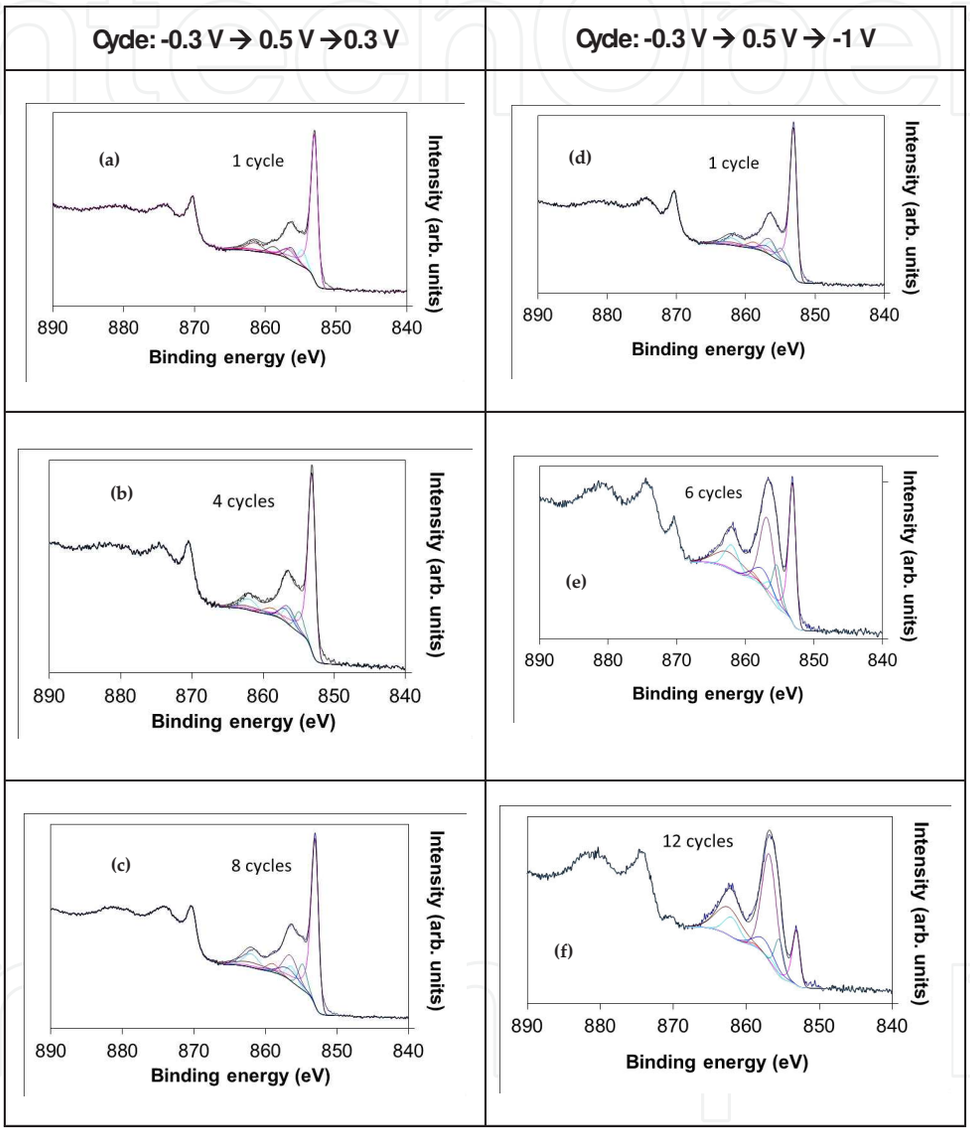

Figure 8. XPS Ni $2p_{3/2}$ core level peak decompositions of a Ni electrode immersed in carbonate buffer saline solution (pH 6.4), in presence of 120 mM NaCl, for different numbers of cycles in different potential range [adapted from 21].

In a restricted anodic potential range, XPS results indicate that the surface was passivated by a 1 nm-thick duplex layer composed of nickel hydroxide (outermost layers) and nickel oxide (inner layers). In a negative extended potential range, though the electrochemical behavior of electrodes did not change, the inner nickel oxide layer was thickening, indicating a surface degradation of the nickel electrode in these conditions.

http://dx.doi.org/10.5772/53965

Sample treatment	NiO equivalent thickness (nm)	$Ni(OH)_2$ equivalent thickness (nm)	Passive layer thickness (nm)
-0.3 V→ 0.5 V→ -0.3V	with 120 mM NaCl		
1 cycle	0.7 ± 0.1	0.5 ± 0.1	1.2 ± 0.2
4 cycles	0.7 ± 0.1	0.7 ± 0.1	1.4 ± 0.2
8 cycles	0.9 ± 0.1	0.7 ± 0.1	1.6 ± 0.2
-0.3V→ 0.5 V→ -1.0 V	with 120 mM NaCl		
1 cycle	0.5 ± 0.1	0.8 ± 0.1	1.3 ± 0.2
6 cycles	1.4 ± 0.1	1.3 ± 0.1	2.7 ± 0.2
12 cycles	2.6 ± 0.1	1.4 ± 0.1	4.0 ± 0.2
-0.3V→ 0.5 V→ -1.0 V	without 120 mM NaCl		
1 cycle	0.7 ± 0.1	1.0 ± 0.1	1.7 ± 0.2
6 cycles	1.8 ± 0.1	1.1 ± 0.1	2.9 ± 0.2
12 cycles	2.3 ± 0.1	1.8 ± 0.1	4.1 ± 0.2

Table 1. NiO and $Ni(OH)_2$ layer thicknesses estimated from the XPS Ni $2p_{3/2}$ core level peak decompositions (two-layer model) [adapted from 21].

These systematic observations, in different potential ranges, show that alternating the polarity of the electrodes ensures the reproducibility of measurements for a large number of clinical tests and explain why, during routine use of the medical device, the metal/sweat interaction may reduce the lifetime of the anodic and/or cathodic electrodes.

4.5. Stainless-steel electrodes behavior: Comparison with nickel

Although the contact duration of nickel with skin is only about 2 minutes, the risk of allergic reactions cannot be discarded. In order to improve the device, a new electrode material, stainless steel 304L (SS 304L), with lower Ni content, was tested in carbonate buffer solutions in the presence of various concentrations of chloride, lactate and urea to mimic the chemical composition of the sweat.

Stainless steel 304L (SS 304L), already used in surgical instruments for example, was selected as a potential substitute material. Thus, the electrochemical behavior of SS 304L was analyzed and, more particularly, its sensitivity to the variation of different parameters in sweat. This work is aimed at understanding the adequacy of stainless steel 304L to the clinical testing application. The electrochemical measurements were performed in a three-electrode set up combining a stainless steel 304 L counter electrode in order to mimic the 2 active electrodes configuration (the same material is used for the anode and the cathode) of the SUDOSCAN™ device.

As for nickel, the influence of the variation of electrolyte concentrations on the electrochemical behavior of SS 304L, mainly appears by a deviation of the generated currents at high

anodic voltage potential and notably the deviation of the breakdown potential, E_b, towards less or higher anodic potentials.

The obtained results show that SS 304L is more sensitive than Ni to the variation of Cl^- concentration. Figure 9 shows the cyclic voltammograms recorded on SS 304L in carbonate buffer solutions (36 mM, pH 7) without Cl^- and with increasing concentrations of Cl^- within the expected range of concentrations in sweat at rest. In all cases, the concentration of Cl^- is high enough to cause the destruction of the passive film. Furthermore, E_b decreases with increasing chloride concentration. A high shift of about 0.42 V was observed by varying chloride concentration from 30 to 120 mM at pH 7.

As for nickel, a linear variation between E_b and Log([Cl^-]) was also observed. However, SS 304L is more sensitive than Ni to the variation of Cl^- concentration. The slope value of the linear variation of E_b as a function of Log([Cl^-]) was ≈ 0.2 for Ni and ≈ 0.67 for SS 304L (Figure 10).

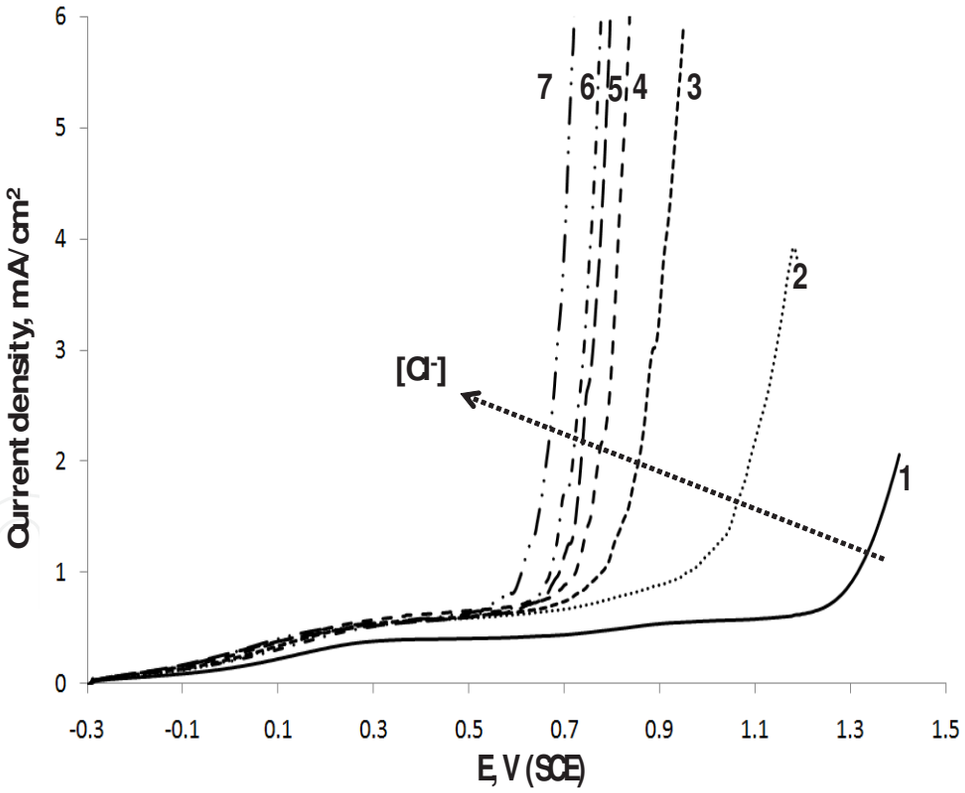

Figure 9. Cyclic voltammograms of SS 304L electrode in aerated CBS (36 mM, pH 7) in presence of NaCl (curve 1: 0 mM; curve 2: 30 mM; curve 3: 45 mM; curve 4: 60 mM; curve 5: 75 mM; curve 6: 90 mM and curve 7: 120 mM). Only the forward scans are shown. Scan rate: 100 mV/s [adapted from 30].

http://dx.doi.org/10.5772/53965

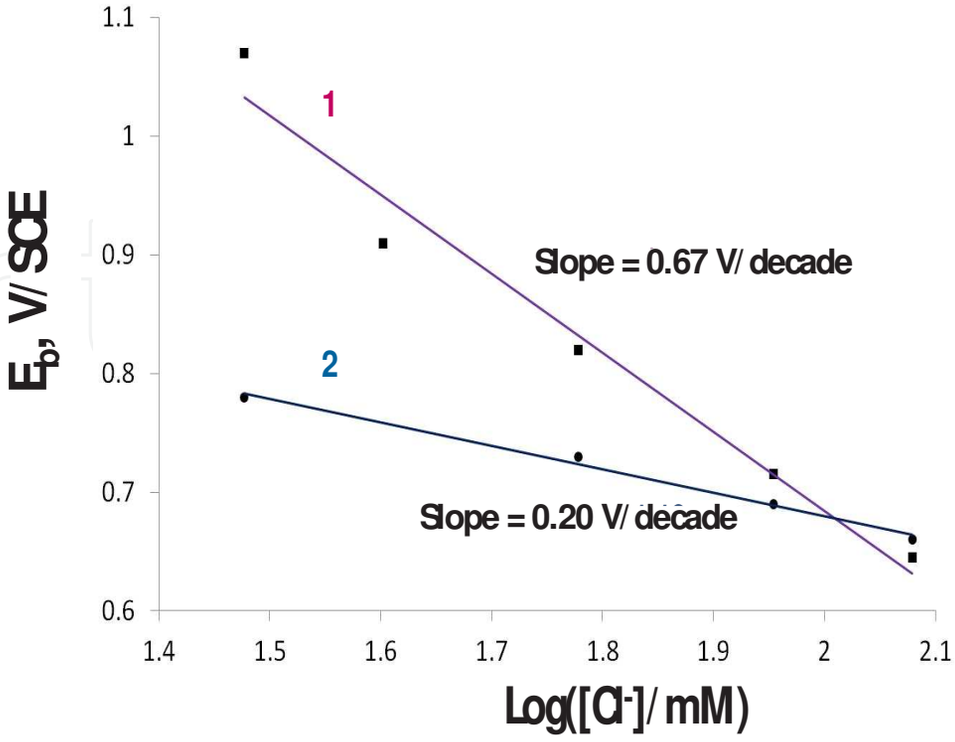

Figure 10. E_b vs. Log [Cl^-]. Data obtained from cyclic voltammograms on (1 : SS 304L electrode; 2 : nickel electrode) in carbonate buffer solutions (36 mM, pH 7) in presence of different concentrations of Cl^- (between 30 and 120 mM).

The effect of adding increasing amounts of Cl^- on E_b of SS 304L in CBS (36 mM) at pH 5, 5.5 and 6 was also examined. Table 2 presents the E_b values deduced from cyclic voltammograms recorded (data not shown) at different pH and chloride ions concentration. It clearly appears that, at pH 5 and 5.5, the localized dissolution occurs only when Cl^- concentration exceeds 40 mM, whilst at pH 6, Cl^- concentration should exceed 30 mM.

[NaCl](mM)	E_b, V_{SCE} (pH 5)	E_b, V_{SCE} (pH 5.5)	E_b, V_{SCE} (pH 6)	E_b, V_{SCE} (pH 7)
0	1.38	1.38	1.34	1.30
30	1.38	1.38	1.31	1.06
40	1.38	1.38	1.15	0.90
60	1.07	1.03	0.92	0.805
90	0.88	0.83	0.79	0.70
120	0.77	0.76	0.73	0.64

Table 2. E_b values deduced from cyclic voltammograms recorded on SS 304L in CBS of different pH and containing various chloride ions concentration [30].

The effect of pH, buffer concentration, urea concentration and lactate concentration was also studied. The obtained results show that variation of pH, buffer concentration and lactate concentration also affect, but to a less extent than chloride, the electrochemical behavior of SS 304L by displacing E_b towards lower or higher anodic potentials [30]. As the variation range of these parameters in sweat is low compared to that of Cl^-, and as the breakdown potential (E_b) is highly shifted by varying Cl^- concentration, the currents obtained during the clinical tests are likely to be controlled by the variation of Cl^- concentration. These results tend to prove that SS 304L is suitable for use in the SUDOSCAN™ application due to its high capacity to detect the deviation in the ionic balance and notably the deviation in Cl^- concentration.

5. Conclusion

The study of the electrochemical behavior of nickel was carried out in sweat-mimic solutions and using a set-up similar to that of the medical device. This study allowed us to define the origin of the onset of responses measured upon the application of low voltage potential with variable amplitudes to Ni electrodes. This study also clearly indicates that the variation of chloride concentration is the main sweat parameter controlling the electrochemical currents.

The comparisons between *in-vitro* study and clinical observations clearly indicate that the electrochemical *in-vitro* measurements on the behavior of nickel electrodes are close enough to those obtained through the clinical tests and prove that the determination of the current curve as a function of the potential (anode, cathode or their difference) provides a very efficient way to detect the deviation in Cl^- concentration, at the level of the electrodes.

The influence of chloride concentrations on the kinetics of the electrochemical reactions was also studied. The proposed mechanisms and the obtained kinetic parameters were then used by Impeto Medical to complete a theoretical model.

An evaluation of the ageing of electrodes on their performance was conducted by realizing surface analyzes, such as XPS and SIMS spectroscopies. Our results have highlighted the importance of alternating the polarity of electrodes to ensure their sensitivity and the reproducibility of measurements. However, after frequent uses, the metal/sweat interaction can lead to a slight deterioration of the electrodes surface.

Finally, in order to reduce the allergic risk, the electrochemical studies were extended to the stainless steel 304L as a replacement material of nickel. The electrochemical study shows that stainless steel 304L is very sensitive to the deviation of sweat ionic balance and notably to the variation of chloride concentrations at the level of electrodes. This makes stainless steel 304L a very promising material for the medical device application.

Results obtained from *in-vitro* studies have been used to improve the development of EZSCAN/SUDOSCAN.

http://dx.doi.org/10.5772/53965

In perspective, it could be interesting to compare the electrochemical behavior and surface modification between electrodes aged in-vivo and electrodes aged *in-vitro* and to study the electrochemical behavior of different compositions of stainless steel. It could be also interesting to study the electrochemical kinetics of anodic reactions taking place at the surface of stainless steel electrode in physiological solutions.

Author details

Hanna Ayoub[1,2,3], Jean Henri Calvet[3], Virginie Lair[1*], Sophie Griveau[2], Fethi Bedioui[2] and Michel Cassir[1]

1 LECIME CNRS UMR 7575, Chimie ParisTech, Paris, France

2 UPCGI CNRS 8151/INSERM U 1022, Université Paris Descartes, Chimie ParisTech, Paris, France

3 IMPETO Medical, Paris, France

References

[1] IDF, Diabetes Atlas Fifth Edition. Diabetes Atlas ed. IDF. Brussels: International Diabetes Federation 5 (2011)

[2] American Diabetes Association. Diagnosis and classification of diabetes mellitus. Diabetes Care 33 (2010) 62

[3] Tesfaye S, Boulton AJ, Dyck PJ, Freeman R, Horowitz M, Kemper P et al. Diabetes Care 33 (2010) 2285

[4] Low VA, Sandroni P, Fealey RD, Low PA. Muscle Nerve 34 (2006) 57

[5] Lauria G, Cornblath DR, Johansson O, McArthur JC, Mellgren SI, Nolano M, et al. Eur J Neurol 12 (2005) 1

[6] Knowler WC, Barrett-Connor E, Fowler SE, et al. Diabetes Prevention Program Research Group. Reduction in the incidence of type 2 diabetes with lifestyle intervention or metformin N Engl J Med 346 (2002) 393.

[7] Brunswick P, Bocquet N, Patent number: France 0753461 and PCT EP2008/052211.

[8] Schwarz P, Brunswick P, Calvet JH. Journal of Diabetes & Vascular diseases 11(2011) 204.

[9] Bland JM, Altman DG. Lancet 327 (1986) 307.

[10] Gin H, Baudouin R, Raffaitin C, Rigalleau V, Gonzalez C. Diabetes & Metabolism 11(2011) 527.

[11] Calvet JH, Dupin J, Deslypere JP. Journal of Diabetes & Metabolism. Accepted for publication.

[12] Ozaki R, Cheung KKT, E. Wu, A. Kong, X. Yang, E. Lau, P. Brunswick, JH. Calvet, JP.Deslypere, J.C.N. Chan. Diabetes technology & therapeutics 13 (2011) 937.

[13] Hubert D, Brunswick P, Calvet JH, Dusser D, Fajac I. Journal of Cystic Fibrosis 10 (2011)15.

[14] Ramachandran A, Moses A, Snehalatha C, Shetty S, Thirupurasundari CJ, Seeli AC. Journal of Diabetes & Metabolism 2 (2011)1.

[15] Ayoub H, Griveau S, Lair L, Brunswick P, Cassir M, Bedioui F. Electroanalysis 22 (2010) 2483.

[16] Milosev I, Kosec T, Electrochimica Acta 52 (2007) 6799.

[17] Real SG, Barbosa MR, Vilche JR, Arvia AJ, Journal of Electrochemical Society 137 (1990) 1696.

[18] Khalfallah K, Ayoub H, Calvet JH, Neveu X, Brunswick P, Griveau S, Lair V, Cassir M, Bedioui F. IEEE Sensors Journal 12 (2012) 456.

[19] Ayoub H, Lair V, Griveau S, Brunswick P, Bedioui F, Cassir M. Sensors Letters Journal 9, (2011) 2147.

[20] Ayoub H, Lair V, Griveau S, Brunswick P, Zagal J H, Bedioui F, Cassir M. Electroanalysis, 24 (2012) 386.

[21] Ayoub H, Lair V, Griveau S, Galtayries A, Brunswick P, Bedioui F, Cassir M. Applied Surface Science 258, (2012) 2724.

[22] Hoar TP. Corrosion Science 7 (1967) 341.

[23] Burke LD, Whelan DP, Electroanal J. Chem. 109 (1980) 385.

[24] Burke LD, Twomay TAM. J. Electroanal. Chem 162 (1984)101.

[25] Laksono E, Galtayries A, Argile C, Marcus P. Surface Science 530 (2003) 37

[26] Payne BP, Grosvenor A P, Biesinger M C, Kobe B A, McIntyre N S. Surf. Interface Anal. 39 (2007) 582.

[27] Biesinger M C, Payne B P, Lau LWM, Gerson A, Smart RStC. Surf. Interface Anal. 41 (2009) 324.

[28] Marcus P, Herbelin J-M. Corrosion Science 34 (1993) 1123.

[29] Marcus P, Oudar J, Olefjord I, Microsc J. Spectr. Electron. 4 (1979) 63.

[30] Ayoub H, Lair V, Griveau S, Brunswick P, Bedioui F, Cassir M. Electroanalysis 24 (2012) 1324.